

COMPARATIVE STUDY OF SUBSYNCHRONOUS ROTATING FLOW PATTERNS  
IN CENTRIFUGAL COMPRESSORS WITH VANELESS DIFFUSERS

P. Frigne\*  
State University of Gent  
9000 - Gent, Belgium

R. Van Den Braembusche  
von Karman Institute  
1640 - Rhode Saint Genèse, Belgium

SUMMARY

A comparative experimental investigation of the unstable operating modes of a centrifugal compressor is made. Hot wire measurements, in two different compressor configurations, allowed to distinguish between the different unsteady flow pattern. Impeller and/or diffuser rotating stall has been observed, depending on the flow conditions. The measured relative rotational speed of this perturbation is cross-checked with other experimental data and it is shown that the rotational speed is strongly dependent on the type of rotating stall. The diffuser absolute inlet flow angle at the onset of diffuser rotating stall agrees well with the value predicted by an existing stability criterion.

INTRODUCTION

Self excited vibrations of turbomachinery components, due to aerodynamic forces, can be divided into two groups. A first one concerns the vibrations where the destabilizing forces are function of the whirling motion of the rotor. The initial displacement of the shaft influences the flow conditions in the labyrinth seals or creates an asymmetric blade loading on the impeller. The corresponding forces sustain the initial perturbation because of the negative damping.

A second type concerns the vibrations where the main flow is destabilized by hydrodynamic or viscous forces which are independent of the resulting mechanical vibration. They are known as rotating stall and surge. The last ones have also an important influence on compressor performance.

At low pressure levels, the corresponding forces are often too small to have any significant influence on the shaft vibrations, but sometimes result in blade failures. However, at high pressure levels the excitation becomes much larger and very often limits the range of operation because of vibrational problems.

This paper is limited to the study of the second type of destabilization in centrifugal compressors with vaneless diffusers.

---

\* Formerly Research Associate at von Karman Institute.

Hot wire measurements have been performed in two different compressor configurations in order to investigate the different unsteady flow pattern.

### SYMBOLS

$b$	diffuser width
$C_p$	static pressure rise coefficient
$i$	number of stall cells
$P$	static pressure
$R$	radius
$Re_{b_2}$	Reynolds number, based on diffuser absolute inlet velocity and diffuser width
$U$	peripheral velocity
$V$	absolute velocity
$\alpha$	absolute flow angle, measured from meridional plane
$\beta$	blade angle measured from meridional plane
$\phi$	mass flow coefficient
$\rho$	static density
$\mu$	slip factor
$\omega_s$	absolute angular velocity of stall cells
$\Omega$	angular velocity of the impeller

### Subscripts

0	settling chamber
1	inducer inlet channel
2	diffuser inlet
3	diffuser outlet
c	critical

## DESCRIPTION OF TEST FACILITY AND INSTRUMENTATION

The experiments have been performed in the open loop test facility (Fig. 1a) of the State University of Gent. Mass flow is fed into the settling chamber by a normalized tube which allows for flow control and mass flow measurement. Inlet guide vanes can be installed in the suction pipe if prerotation is required. Flow is discharged at atmospheric pressure after a 180° turning at the diffuser exit.

All measurements have been performed with a vaneless diffuser. Geometrical parameters of the unshrouded impeller (Fig. 2) are listed in Table 1.

Besides the classical pressure and temperature probes, required for overall performance measurements, four hot wire probes are also installed. The hot wires are mounted perpendicular to the mean flow direction. One is installed at impeller inlet (II), one at diffuser inlet (ID) and two at  $R/R_2 = 1.3$  inside the diffuser (MD1 and MD2) at 42° circumferential distance (Fig. 1b). The linearized signals are visualized on an oscilloscope and processed with a HP 3582A two channel Fourier spectrum analyser. This allows to define the power spectrum, coherence function and phase transfer function.

Perturbations rotating in the diffuser will result in periodic signals at MD1 and MD2 with period  $\tau_2$ . Because of the 42° difference in circumferential position there will be a time lag  $\tau_1$  which allows to calculate the number of stall cells  $i$ , and the rotational speed  $\omega_s$ :

$$i = 360/42 * \tau_1/\tau_2 \quad (i \text{ must be integer})$$

$$\omega_s = 2\pi/(i\tau_2).$$

## TEST RESULTS WITHOUT PREROTATION VANES

The first series of measurements have been obtained with an axial flow at compressor inlet. The overall performances are shown on figure 3. The static pressure rise is not related to the mass flow coefficient  $\phi_2$  but to the diffuser inlet flow angle  $\alpha_2$ . The last parameter is used here because of its important influence on diffuser stability and is defined by

$$\text{tg } \alpha_2 = \mu/\phi_2.$$

The slip factor is calculated from correlations and is checked against the measured impeller temperature rise. Increasing values of  $\alpha_2$  correspond to decreasing mass flow.

The static pressure rise is non dimensionalized by  $\rho_0 U_2^2/2$  to become independent of RPM.

All curves show a maximum at  $\alpha_2 = 76^\circ$  which coincides with the onset of unstable flow. At higher RPM, these curves do not continue to the left because of surge. At low RPM, surge occurs only at  $\alpha_2 = 87^\circ$

which leaves a large range of flow conditions where unsteady flow can be observed. The hot wire measurements are therefore made at 2000 RPM for  $\alpha_1$  values between  $76^\circ$  and  $87^\circ$ .

The hot wire traces shown on figure 4a are measured at rotor inlet (II) and diffuser inlet (ID) for  $\alpha_2 = 76^\circ$ . The relative amplitude of the oscillations, defined by  $(V_{\max} - V_{\min})/V_{\text{RMS}}$ , amounts to .14 at rotor inlet and .23 at diffuser inlet. The power spectrum and coherence function, shown on figures 4b and 4c, clearly indicate an instability at 27.2 Hz. Inside the diffuser, at  $R/R_2 = 1.3$ , the flow is steady as shown on the power spectrum of probe MD1 (Fig 4d). One can therefore conclude that these instabilities are due to impeller rotating stall, which can be explained by the high positive incidence ( $12^\circ$ ) at inducer tip for this operating point.

Measurements at  $\alpha_2 = 78^\circ$  (Fig. 5a) do not only show an increase in amplitude to .37 at impeller inlet (II), but also an extension of these perturbations downstream inside the diffuser (MD). The hot wire traces MD1 and MD2 (Fig. 5b) have a relative amplitude of .13. The phase lag between both signals indicates the presence on one stall cell rotating at 77% of the rotor speed. The power spectrum and coherence function of the II and MD signal (Figs. 5c, 5d) reveal a decrease of the basic frequency to 25.6 Hz and the presence of important harmonics at 52 and 77 Hz.

Figures 6a and 6b are measured at  $\alpha_2 = 81^\circ$  and indicate a further increase in amplitude to 200% at rotor inlet (II) and 18% inside the diffuser (MD). The basic frequency is now 23.2 Hz and  $\omega_s/\Omega = .70$ . The harmonics have almost disappeared at rotor inlet but are unchanged inside the diffuser.

Low frequency oscillations completely suppress impeller rotating stall at  $\alpha_2 = 87^\circ$ . The hot wire traces of figure 7a seem to indicate that the frequency at rotor inlet (II) is twice the frequency of oscillations inside the diffuser. However, hot wires read only the velocity component perpendicular to the wire and are insensitive to a  $180^\circ$  change in flow direction. The real flow velocity at rotor inlet changes sign (return flow) and is indicated by the dashed line. Both signals are in phase at 6.4 Hz and indicate compressor surge. The power spectrum on figure 7b shows the presence of several harmonic frequencies as well at rotor inlet as inside the diffuser.

This series of measurements show only one type of rotating stall, originating from the rotor. The oscillations are gradually increasing in amplitude and extending downstream inside the diffuser. They are due to one stall cell rotating at high relative velocity.

#### TEST RESULTS WITH INLET PREROTATION VANES

According to a stability criterion, developed by the authors (Ref. 1), vaneless diffuser rotating stall should occur at  $\alpha_2 = 77^\circ$ . However, only impeller rotating stall has been observed in previous experiments. A possible explanation for this disagreement could be

that diffuser rotating stall is completely suppressed by the impeller rotating stall if the latter one starts first.

In order to verify this hypothesis, inlet guide vanes have been installed in the suction pipe, in order to create  $60^\circ$  prerotation at the impeller inlet. Preliminary calculations indicated that this would delay impeller rotating stall at least to  $\alpha_2 = 82^\circ$ . In this way a sufficiently broad margin for diffuser rotating stall would be created.

The overall compressor performance map is shown on figure 8. Compared to previous results, one can observe a  $6^\circ$  shift to the left of impeller characteristics. The maximum compressor pressure rise has slightly decreased because of the prerotation. The diffuser pressure rise is almost unchanged.

First instabilities are observed in the diffuser at  $\alpha_2 = 77^\circ$  (Fig. 9a). The frequency is 17.6 Hz (Fig. 9b) with a coherence of 55% (Fig. 9c). From the  $132^\circ$  phase shift between MD1 and MD2, one can calculate that three stall cells are rotating at  $\omega_s/\Omega = .176$ . These instabilities are not observed at the inducer inlet (Fig. 9d) and one can therefore conclude that they are due to diffuser rotating stall.

These instabilities have a maximum amplitude of .11 at  $\alpha_2 = 78^\circ$  but completely disappear at  $\alpha_2 = 80^\circ$ . They suddenly reappear in the diffuser at  $\alpha_2 = 80^\circ 5$  with a relative amplitude of .14 and a coherence of 98%.

With the achieved prerotation, the critical flow angle for impeller rotating stall is predicted at  $\alpha_2 = 82^\circ$ . This is experimentally verified by the power spectra obtained at  $\alpha_2 = 82^\circ 6$ . The power peak at 23.2 Hz is measured at rotor inlet and inside the diffuser. The phase angle of  $52^\circ$  indicates that one stall cell rotates at  $\omega_s/\Omega = .673$ . These results are very similar to impeller rotating stall observed with zero prerotation. The power peak at 19.2 Hz is observed only inside the diffuser and the phase angle between MD1 and MD2 indicates that three stall cells are rotating at  $\omega_s/\Omega = .192$ . In analogy to the measurements at lower  $\alpha_2$  values, one can conclude that this is diffuser rotating stall.

When closing the throttle valve further to  $\alpha_2 = 83^\circ 1$ , diffuser rotating stall remains unchanged, but impeller rotating stall (23.2 Hz) disappears completely (Fig. 11).

A new type of unstable flow, with a frequency of 8.8 Hz is observed at  $\alpha_2 = 83^\circ 6$  (Fig. 12a). These instabilities are observed only in the diffuser and correspond to a second type of diffuser rotating stall. Two stall cells are rotating at  $\omega_s/\Omega = 13.2\%$ . These high and low frequency diffuser rotating stall patterns do not occur simultaneously but in a rather intermittent mode. This relative amplitude increases further to .22 at  $\alpha_2 = 84^\circ 7$  (Fig. 12b).

The low frequency oscillations (6.4 Hz), observed at  $\alpha_2 = 86^\circ$ , are in phase and due to compressor surge. Rotating stall has disappeared at this point.

### COMPARISON OF THE TWO TEST SERIES

Impeller rotating stall can be observed at impeller inlet and inside the diffuser. In both test series, the onset of this type of stall coincides with a  $12^\circ$  positive incidence at impeller tip. Pre-rotation therefore allows to delay this type of instability to lower mass flow coefficients.

Diffuser rotating stall can only be observed in the diffuser and starts at  $\alpha_2 = 77^\circ$ . This value will be compared to other data in the next chapter.

Both types of rotating stall can exist simultaneously if diffuser rotating stall occurs first. This absolute frequency and amplitude is of the same order of magnitude and measurements with one single probe do not allow to distinguish between them. However, the relative rotational speed is quite different as shown in figure 13.

Impeller rotating stall has a relative rotational speed of about .7 and this velocity seems to be unaffected by prerotation. The relative rotational speed of diffuser rotating stall is of the order of .10 to .20 only. This difference is in agreement with experimental observations of Lenneman & Howard (Ref. 2), Misuki et al. (Ref. 3) and Abdelhamid (Ref. 4). This difference could therefore be used to distinguish between impeller and diffuser rotating stall. However, the definition of relative rotational speed not only requires to measure the absolute frequency but also the phase difference between two circumferential positions.

### THEORETICAL PREDICTIONS OF VANELESS DIFFUSER ROTATING STALL

Several stability criteria for vaneless diffusers have been developed and published in the literature. They are based on different assumptions and result in contradictory conclusions.

The stability criterion for vaneless diffusers of C. Rodgers (Ref. 5) is based on theoretical considerations concerning variation of  $C_p$  in function of  $\alpha_2$ . The critical value of  $\alpha_{2c}$ , separating the zone of stable operation from the unstable zone, is function of the non dimensionalized diffuser width  $b_2/R_2$  and radius ratio  $R_3/R_2$ .

This conclusion is similar to the one obtained by W. Jansen (Ref. 6). His criterion is based on detailed calculations of the viscous flow in vaneless diffusers. Besides diffuser width ( $b_2/R_2$ ), radius ratio ( $R_3/R_2$ ) and flow angle ( $\alpha_2$ ), stability is now also a function of the Reynolds number. Both theories suggest that the critical flow angle  $\alpha_{2c}$  is decreasing for decreasing diffuser width. This

would mean that for a given impeller, an unstable vaneless diffuser cannot always be stabilized by decreasing the diffuser width.

A similar but more precise calculation by Senoo (Ref. 7), however, results in a criterion which shows an opposite trend in terms of  $\alpha_{2c}$  as a function of diffuser width. The critical flow angle is now increasing for decreasing diffuser width. An unstable diffuser can therefore be stabilized by decreasing diffuser width. This theory also allows to draw important conclusions in terms of diffuser radius ratio  $R_3/R_2$  and about the influence of non uniform flow at diffuser inlet.

The stability criterion of A. Abdelhamid (Ref. 8) is based on rotor-diffuser interaction and does not account for viscous effects. This criterion relates stall operation to the pressure and tangential velocity fluctuations non dimensionalized by radial velocity fluctuations. This criterion is not easily applicable and stability is independent of diffuser width.

In order to eliminate the contradiction between the different criteria, the authors (Ref. 1) have performed some unsteady flow measurements on different impeller-diffuser combinations. These results and other experimental data from the literature allowed to derive the following correlation. All values of  $\alpha_{3c}$  fall within a relatively narrow band as shown on figure 14 after they have been corrected for Reynolds number influence according to figure 15. Points 1 to 5 are experimental data obtained by the authors. Points 6 to 16 are derived from published data.

These experimental data indicate an increase of  $\alpha_{3c}$  for decreasing diffuser width and agree very well with the predictions of Senoo. His theoretical results do not indicate an influence of Reynolds number on diffuser stability for values of  $b_2/R_2 < .10$ . However, the experimentally observed variation of  $\alpha_{2c}$  in function of Reynolds number is in agreement with the predictions of Jansen ( $\Delta\alpha_2 = 6^\circ =$  between  $Re_{b_2} = 10^4$  and  $Re_{b_2} = 10^5$ ).

The flow angles 1 to 16, are calculated from measured temperature rise and slip factor correlations. Therefore, some doubt could exist about the precision by which these angles are defined. Some special tests have been performed in order to evaluate this error. They are made for one impeller-diffuser combination at two different Reynolds numbers. Flow angles at diffuser inlet are measured by a crossed hot wire. The experimental values shown by points 17 and 18 are already corrected for Reynolds number influence.

The observed differences with the theoretical curve are within an acceptable tolerance and therefore provide an additional verification of this correlation.

Point 19 is the value obtained from the present test series and confirms the stability limit for diffuser rotating stall.

## CONCLUSION

Measurements described in this paper allow to distinguish between impeller or diffuser rotating stall. The onset of impeller rotating stall can be related to inducer incidence and the relative rotational speed is about .70. Diffuser rotating stall is a function of diffuser inlet air angle and Reynolds number and has a relative rotational speed of .1 to .2.

These experiments provide a criterion to distinguish between both phenomena and indicate which part of the compressor should be modified to achieve stable operation.

Flow conditions at the onset of diffuser rotating stall have been compared with a criterion for diffuser stability and agree very well.

## REFERENCES

1. VAN DEN BRAEMBUSSCHE, R.; FRIGNE, P.; ROUSTAN, M.: Rotating non uniform flow in radial compressors. AGARD CP 282, pp 12-1 to 12-14.
2. LENNEMAN, E. & HOWARD, J.H.G.: Unsteady flow phenomena in rotating centrifugal impeller passages. ASME Transact., Series A : J. Engineering for Power, Vol. 92, No. 1, January 1970, pp 65-72.
3. MISUKI, S.; KAWASHIMA, Y.; ARIGA, I.: Investigation concerning rotating stall and surge phenomena within centrifugal compressor channels. ASME Paper 78 GT 9.
4. ABDELHAMID, A.N.: Effects of vaneless diffuser geometry on flow instability in centrifugal compressor systems. ASME Paper 81 GT 10.
5. RODGERS, C.: Impeller stalling as influenced by diffusion limitations. ASME Transact., Series I : J. Fluids Engineering, Vol. 99, No. 1, March 1977, pp 84-97.
6. JANSEN, W.: Rotating stall in radial vaneless diffusers. ASME Transact., Series D : J. Basic Engineering, Vol. 86, No. 6, December 1964, pp 750-758.
7. SENOO, Y. & KINOSHITA, Y.: Limits of rotating stall and stall in vaneless diffuser of centrifugal compressors. ASME Paper 78 GT 19.
8. ABDELHAMID, A.N.: Effects of vaneless diffuser geometry on flow instability in centrifugal compression systems. ASME Paper 81 GT 10

9. LIGRANI, P.M.; VAN DEN BRAEMBUSSCHE, R.; ROUSTAN, M.: Rotating stall measurements in the vaneless diffuser of a radial flow compressor. ASME Paper 82 GT 257

TABLE 1. - GEOMETRICAL CHARACTERISTICS OF THE COMPRESSOR

tip $R_1$	= .095	$b_3$	= .016 m
hub $R_1$	= .054 m	N	= 20
$R_2$	= .208 m	tip $\beta_1$	= 50°
$R_3$	= .400 m	hub $\beta_1$	= 32°
$b_2$	= .016 m	$\beta_2$	= 0°

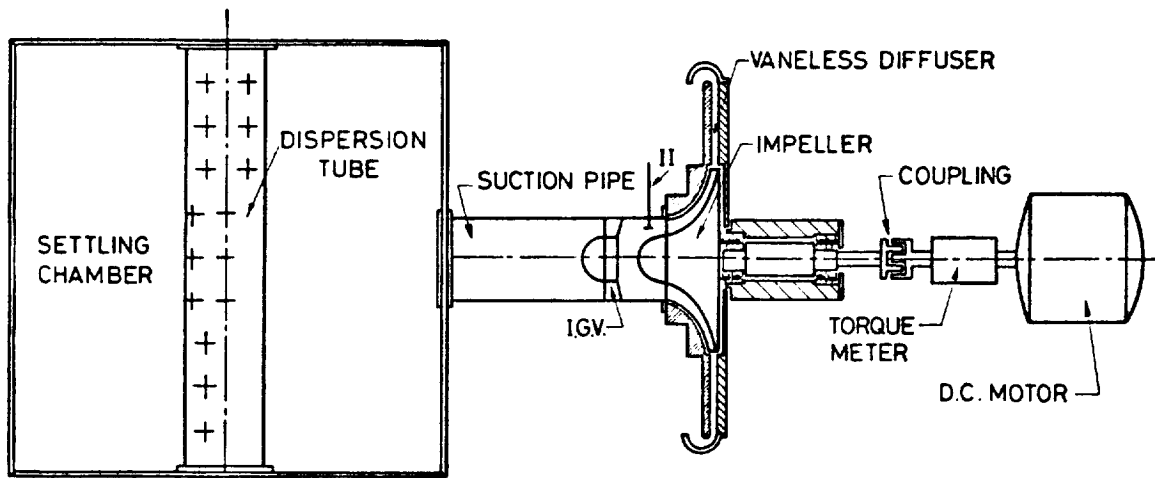


Figure 1(a). - Open loop centrifugal compressor facility.

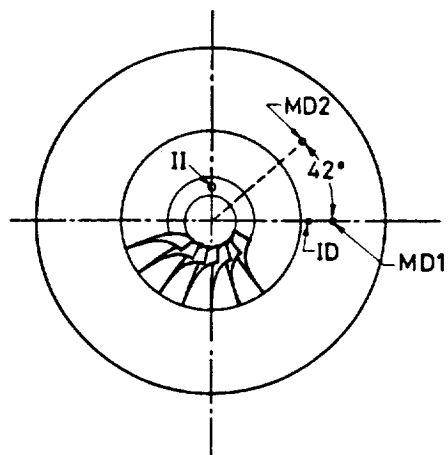
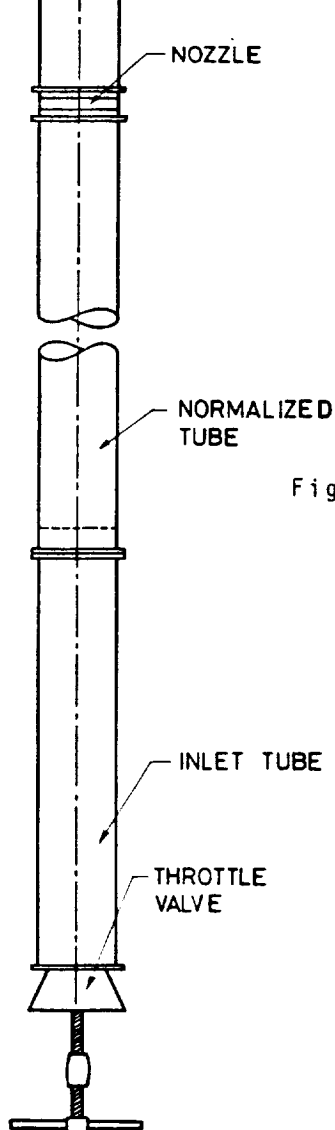


Figure 1(b). - Hot wire locations.

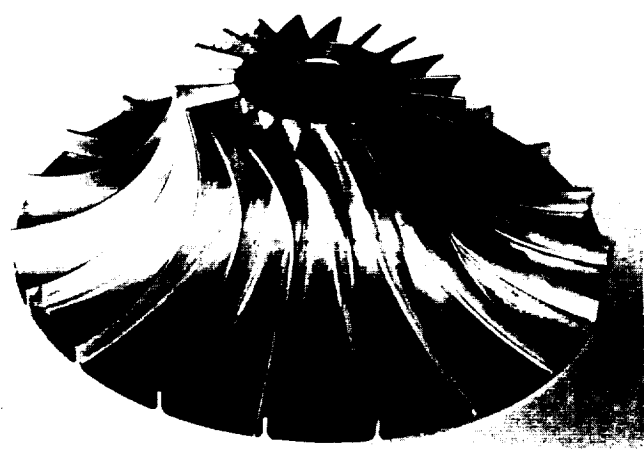


Figure 2. - Unshrouded impeller.

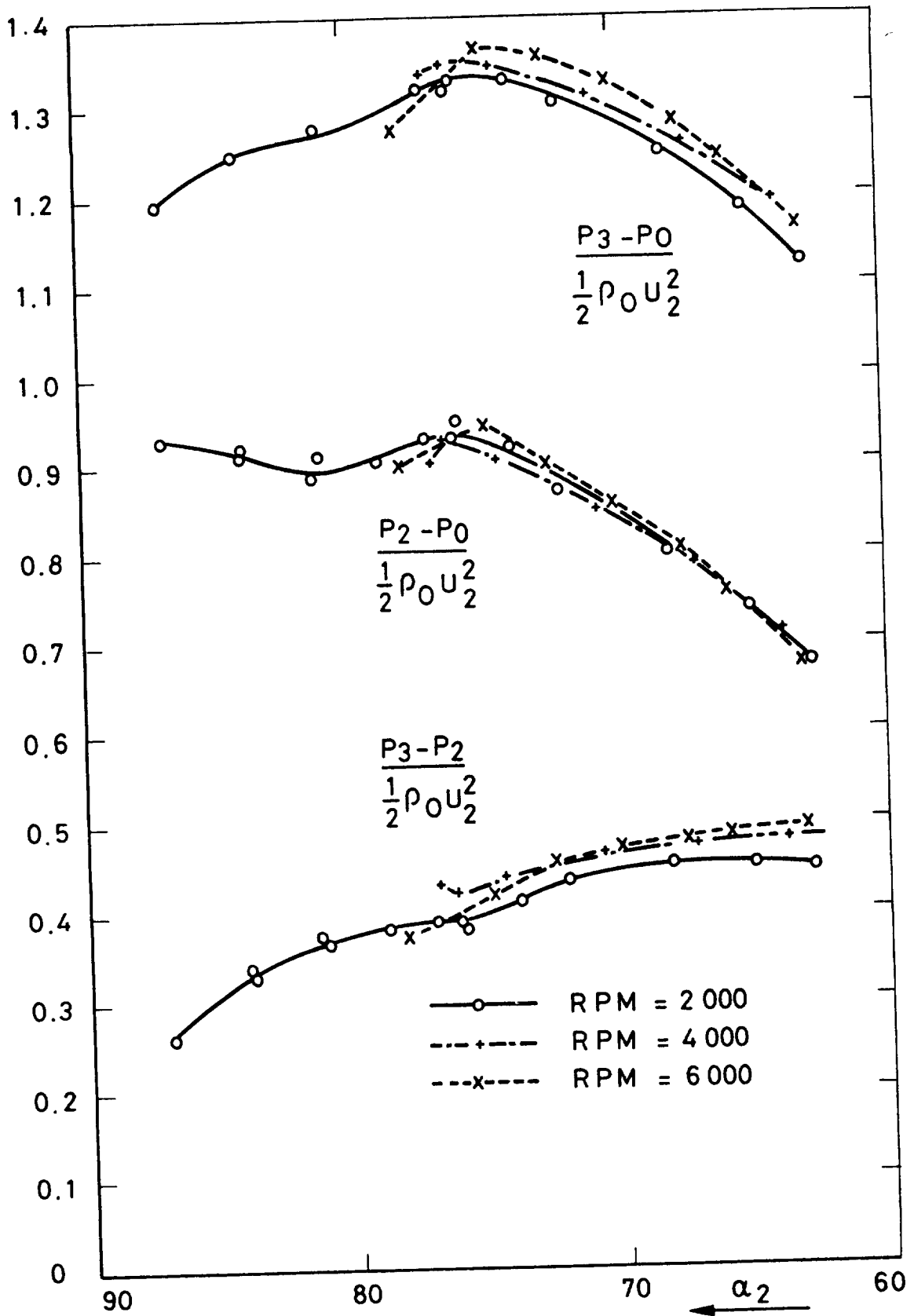


Figure 3. - Compressor performance with zero prerotation.

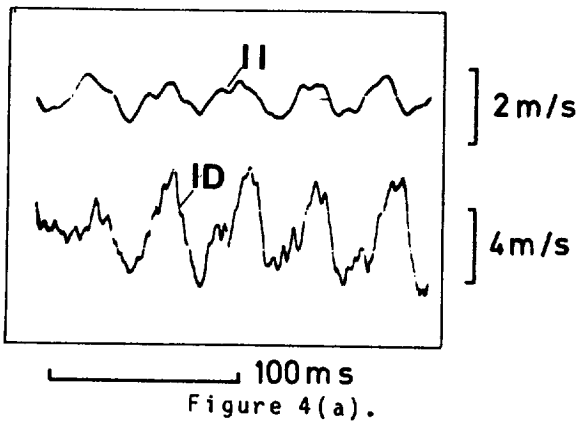


Figure 4(a).

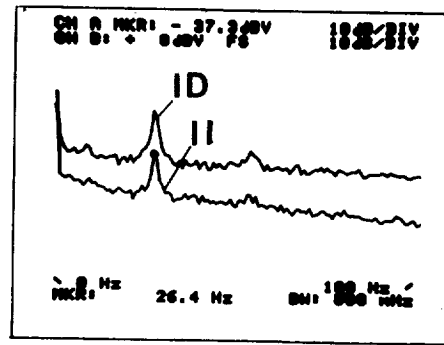


Figure 4(b).

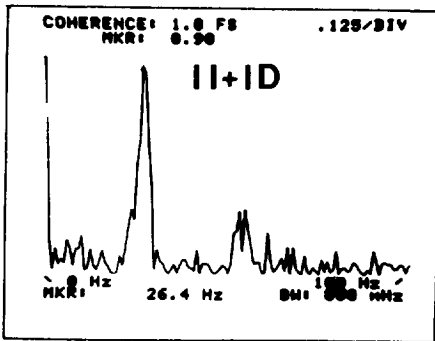


Figure 4(c).

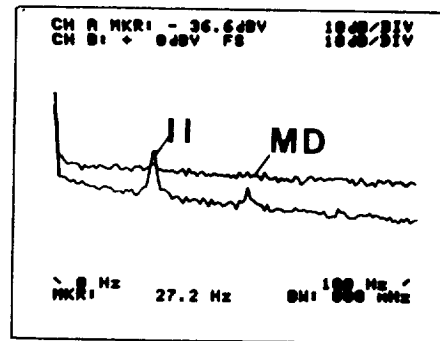


Figure 4(d).

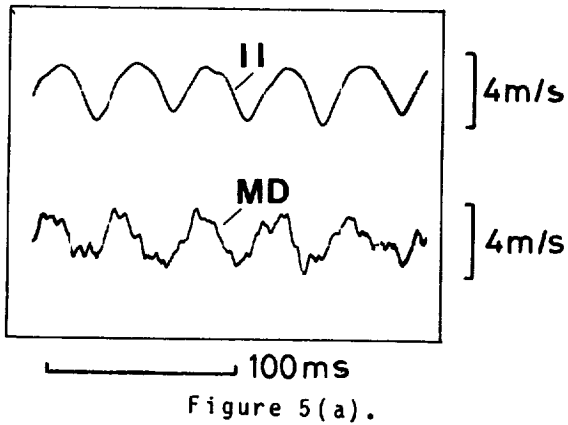


Figure 5(a).

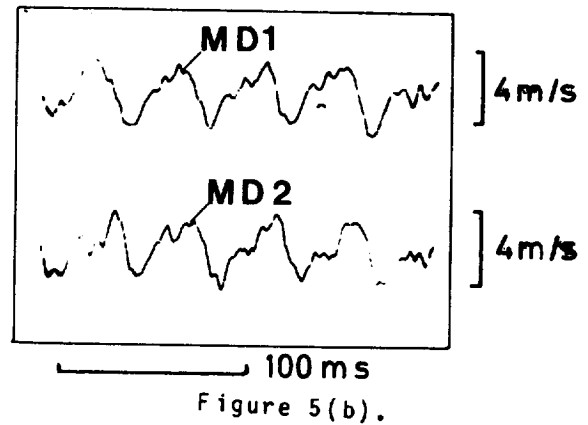


Figure 5(b).

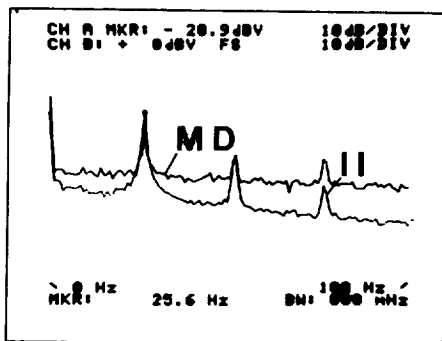


Figure 5(c).

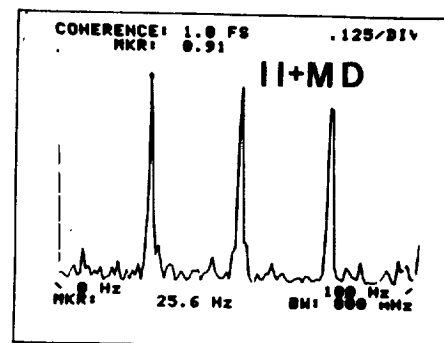


Figure 5(d).

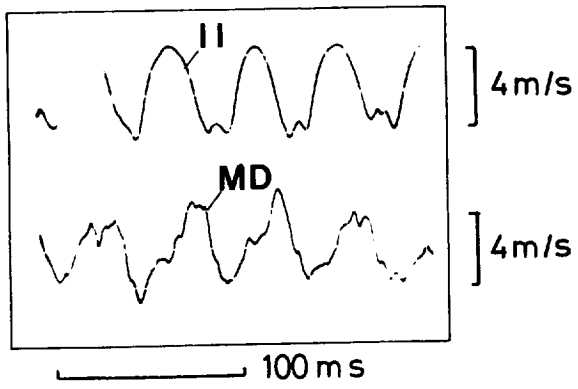


Figure 6(a).

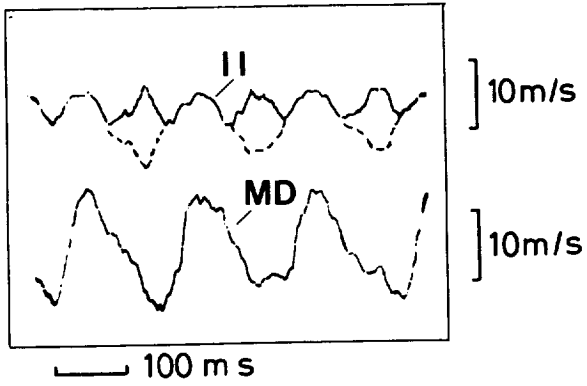


Figure 7(a).

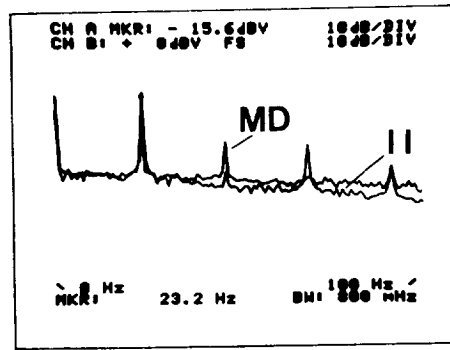


Figure 6(b).

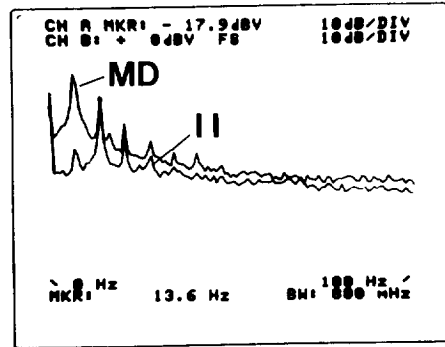


Figure 7(b).

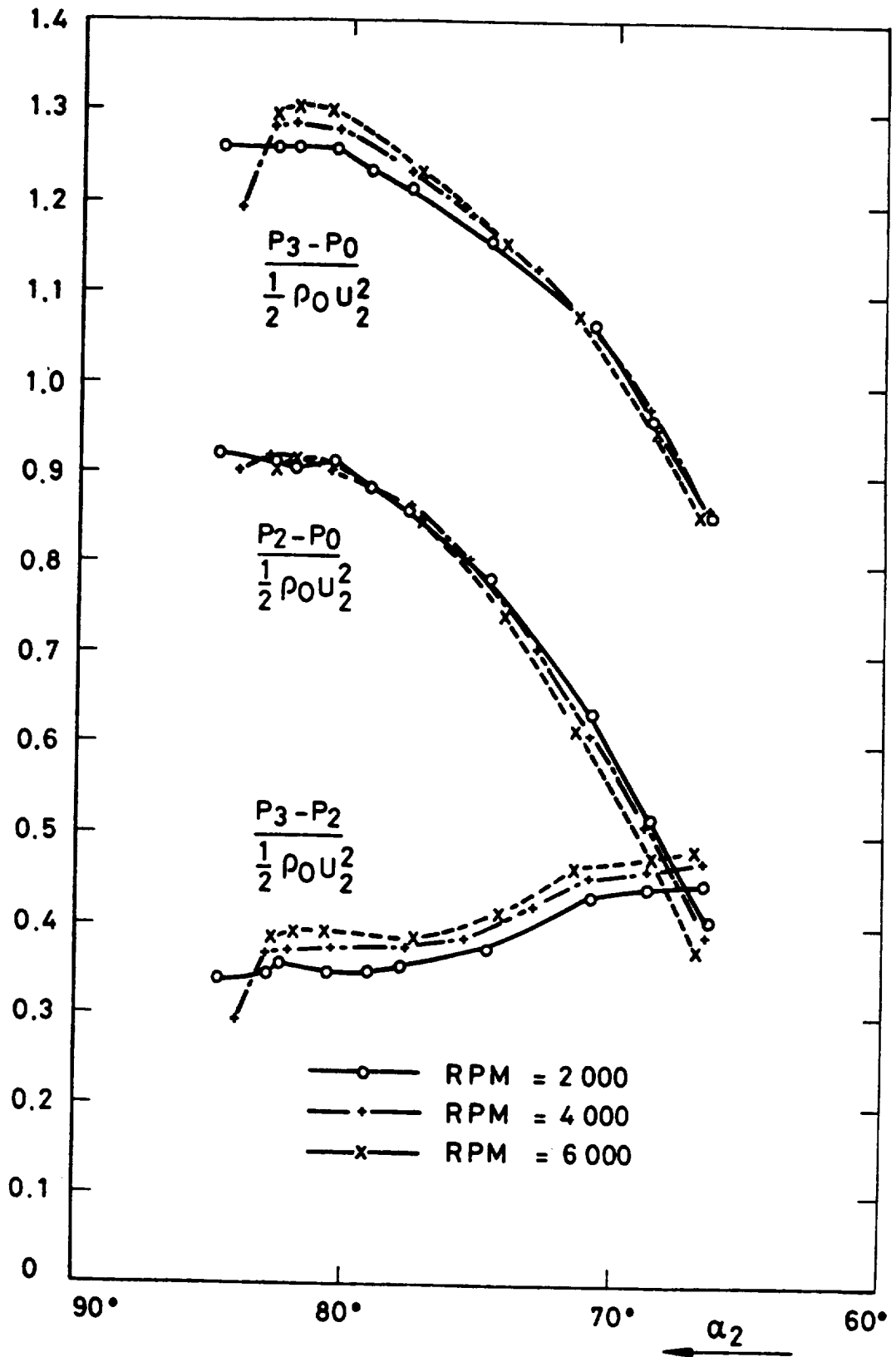


Figure 8. - Compressor performance with 60° prerotation at the inducer tip.

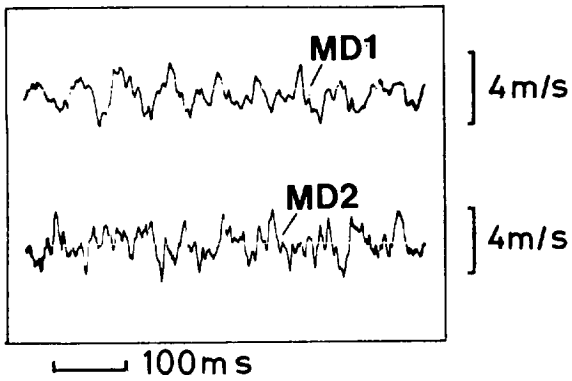


Figure 9(a).

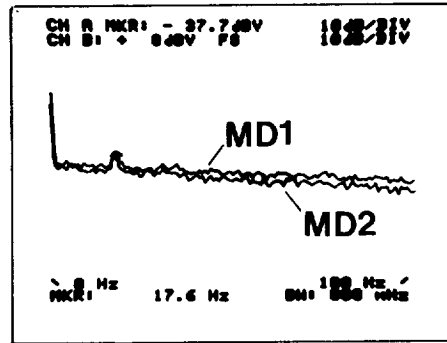


Figure 9(b).

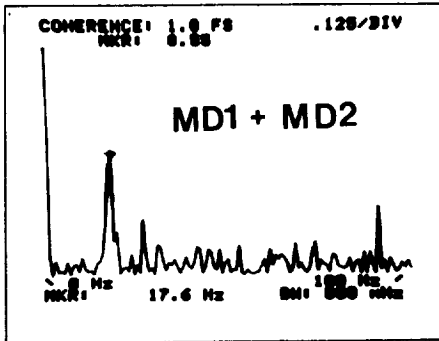


Figure 9(c).

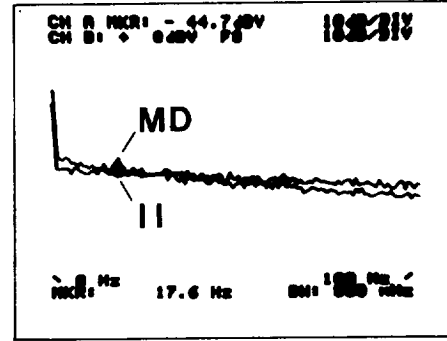


Figure 9(d).

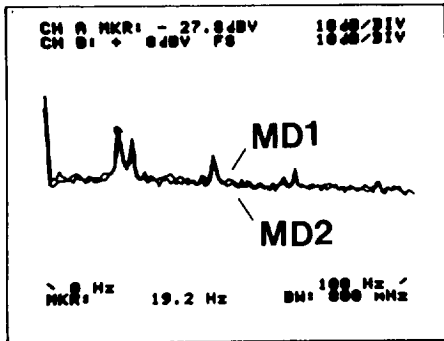


Figure 10(a).

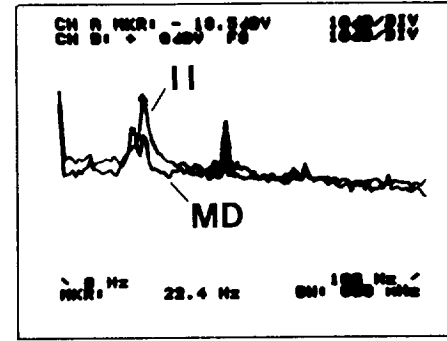


Figure 10(b).

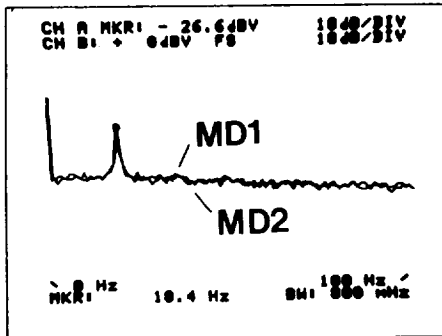


Figure 11.

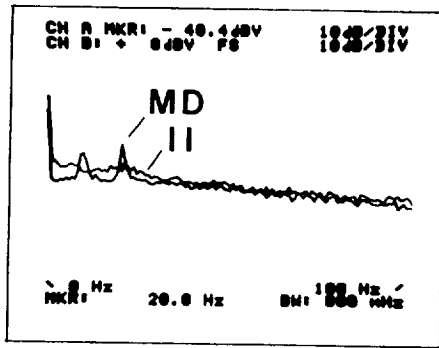


Figure 12(a).

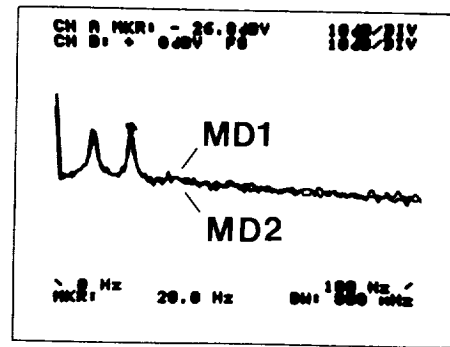


Figure 12(b).

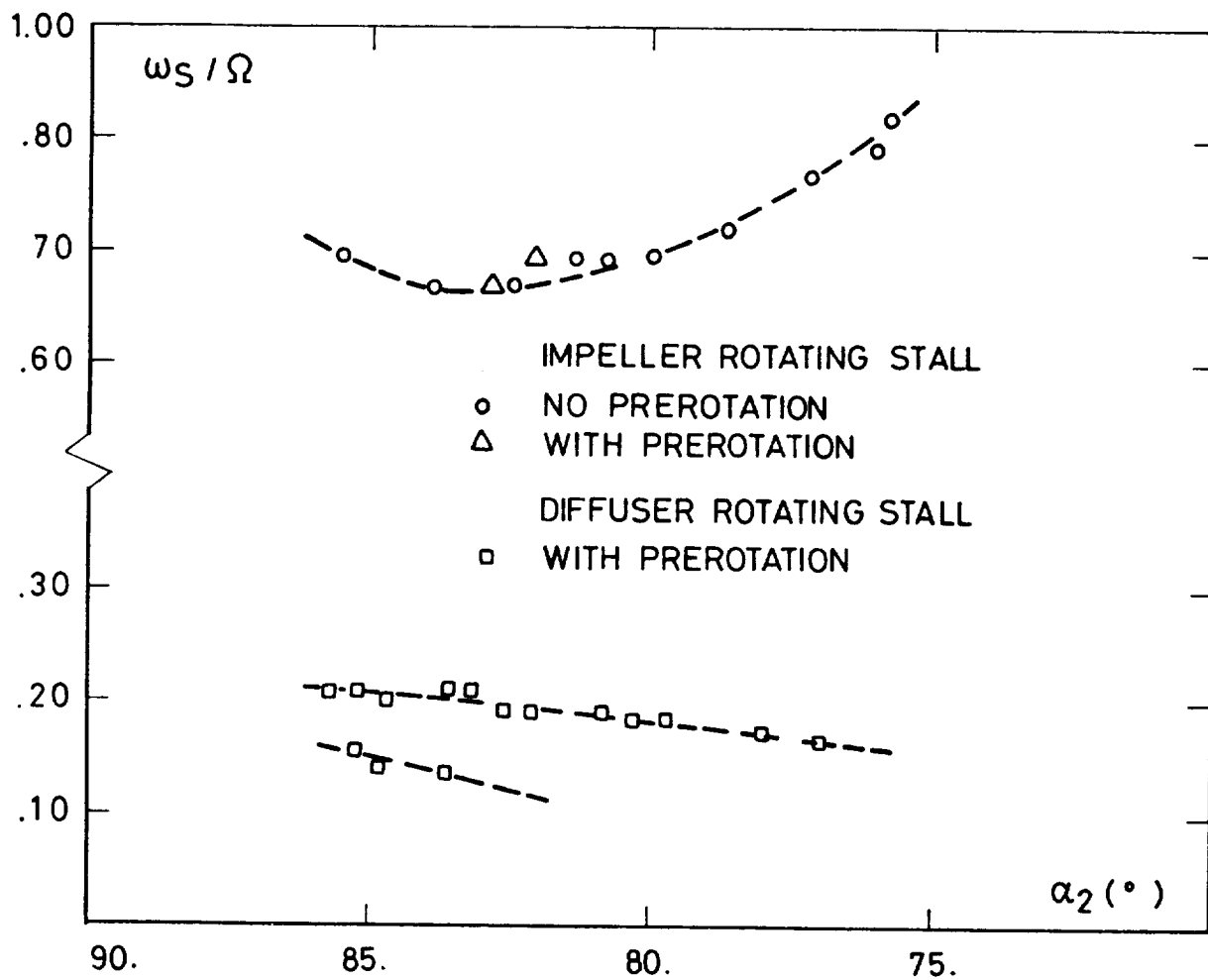


Figure 13. - Relative rotational speed.

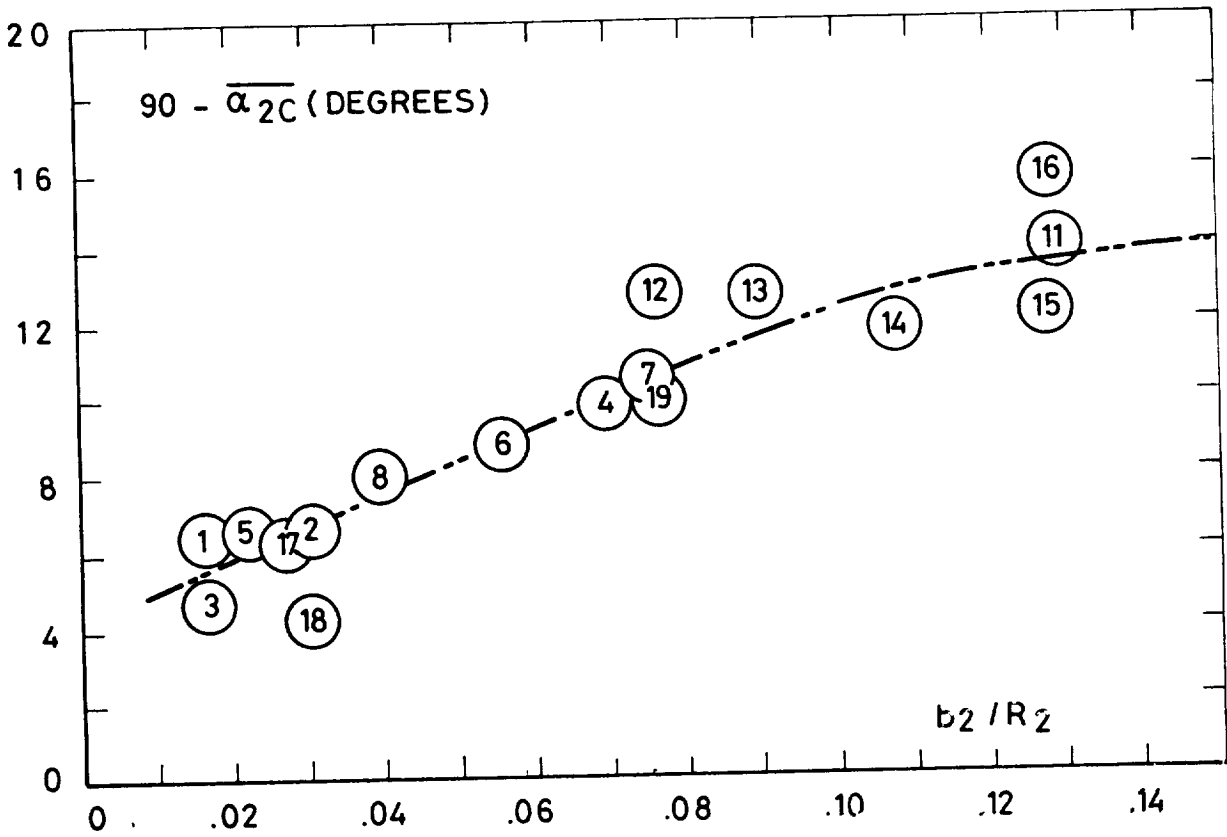


Figure 14. - Critical inlet flow angle complement versus nondimensional diffuser width.

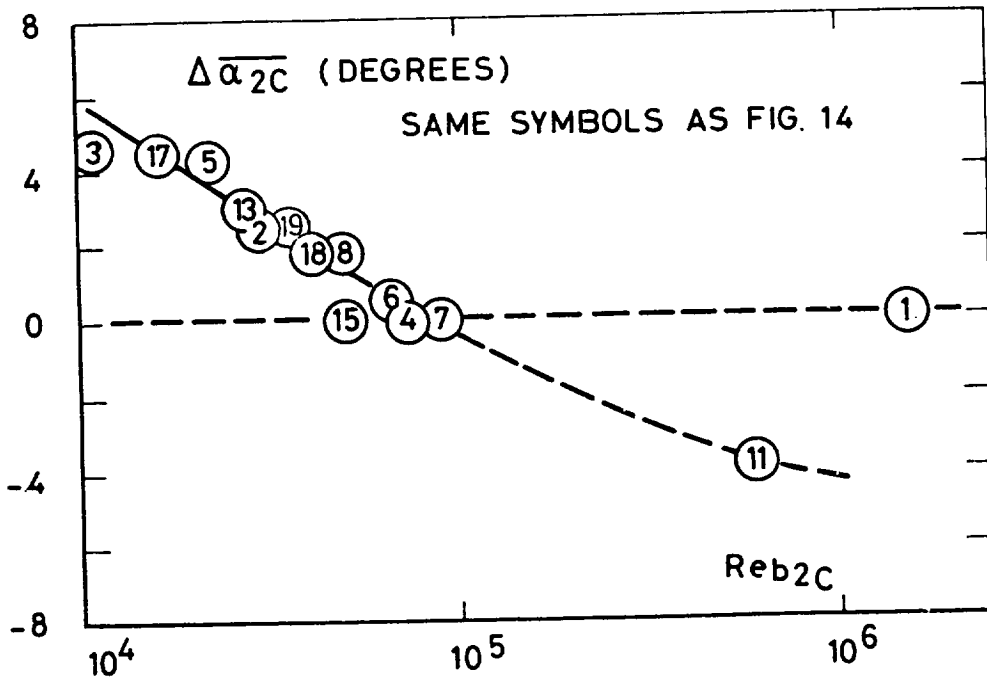


Figure 15. - Critical inlet flow angle correction factor versus Reynolds number.